Intermolecular potentials and the accurate prediction of the thermodynamic properties of water

I. Shvab and Richard J. Sadus[a)]
Centre for Molecular Simulation, Swinburne University of Technology, PO Box 218, Hawthorn, Victoria 3122, Australia

(Received 16 July 2013; accepted 4 November 2013; published online 21 November 2013)

The ability of intermolecular potentials to correctly predict the thermodynamic properties of liquid water at a density of 0.998 g/cm^3 for a wide range of temperatures (298–650 K) and pressures (0.1–700 MPa) is investigated. Molecular dynamics simulations are reported for the pressure, thermal pressure coefficient, thermal expansion coefficient, isothermal and adiabatic compressibilities, isobaric and isochoric heat capacities, and Joule-Thomson coefficient of liquid water using the non-polarizable SPC/E and TIP4P/2005 potentials. The results are compared with both experiment data and results obtained from the *ab initio*-based Matsuoka-Clementi-Yoshimine non-additive (MCYna) [J. Li, Z. Zhou, and R. J. Sadus, J. Chem. Phys. **127**, 154509 (2007)] potential, which includes polarization contributions. The data clearly indicate that both the SPC/E and TIP4P/2005 potentials are only in qualitative agreement with experiment, whereas the polarizable MCYna potential predicts some properties within experimental uncertainty. This highlights the importance of polarizability for the accurate prediction of the thermodynamic properties of water, particularly at temperatures beyond 298 K. © *2013 AIP Publishing LLC*. [http://dx.doi.org/10.1063/1.4832381]

I. INTRODUCTION

The important role played by water in biological, chemical, physical, and technical processes has been the impetus for many attempts to predict its properties. Historically, predicting the properties of water involved either empirical correlations or equation of state modeling.[1,2] More recently molecular simulation[3] has become arguably the method of choice because of the nexus between underlying intermolecular interactions and observable macroscopic properties. In addition to validating theory, molecular simulation is used increasingly to provide worthwhile predictions to both guide and supplement experimental work.

In general, the use of molecular simulation usually requires the *a priori* postulation of an intermolecular potential to evaluate inter-particle forces or energies. There are many alternative intermolecular potentials for water.[4] The basis of many water potentials is at best semi-empirical, although some progress[5] has been made in developing intermolecular potentials from first principles. The most widely used models are rigid and variants of either the four-site[6] transferable interaction potential (TIP4P) or the three-site simple point charge (SPC, SPC/E) models.[7,8] The appeal of such potentials is computational expedience and in many cases they have provided worthwhile predictions. However, comparisons with experiment are often focused at relatively low temperatures and pressures, with a temperature (T) of 25 °C and a pressure (p) of 1 atm being a popular choice.

Simple intermolecular potentials for water have been evaluated for such properties as viscosities and diffusion,[9–11] dielectric constants,[10–12] and water anomalies.[13,14] In contrast, thermodynamic properties have been much less widely investigated. Molecular simulation of the thermodynamic properties for water, and indeed other molecular systems, reported in the literature[10,15,16] are often confined to quantities such as pressure, energy (E), isochoric (C_V), and isobaric (C_P) heat capacities, whereas properties such as the pressure coefficient (γ_V), thermal expansion coefficient (α_P), isothermal (β_T) and adiabatic (β_S) compressibilities, Joule-Thomson coefficient (μ_{JT}), and the speed of sound (w_o) are much less commonly reported. Vega and Abascal[11] compared 17 properties obtained from the most widely used non-polarizable water models (TIP3P, SPC/E, TIP4P, TIP4P/2005, and TIP5P). The comparison included isobaric heat capacity and compressibility but it was restricted to only a few state points.

Typically only a few properties can be observed directly from a single molecular simulation.[17,18] In practice, the isothermal-isobaric (NpT) ensemble (N denotes number of particles) is used to calculate[13,15] C_p, β_T, α_P, the canonical (NVT) ensemble (V denotes volume) is used[17] for C_V, and μ_{JT} is often calculated[19] in the isobaric-isenthalpic (NpH) ensemble (H denotes enthalpy). However, for molecular simulation calculations it is both inconvenient and time consuming to switch between different ensembles to obtain the desired structures, fluctuations, and response functions. In contrast, Lustig[20] showed that, in principle, it is possible to calculate all thermodynamic state variables from key derivatives obtained directly from either molecular dynamics (MD) or Monte Carlo (MC) simulations. The advantage of Lustig's method is that it allows us to directly obtain all the thermodynamic quantities of a fluid from a single MD simulation.

Recently,[21] Lustig's method for the microcanonical ensemble was used to predict the thermodynamic properties of water over a wide range of temperatures using

a)Electronic mail: rsadus@swin.edu.au

the Matsuoka-Clementi-Yoshimine non-additive (MCYna) potential,[22] which combines the *ab initio* two-body MCY potential[23] with an explicit evaluation of induction forces. In many cases excellent agreement with experiment was obtained, demonstrating the importance of polarization on thermodynamic properties. Nonetheless, from a practical perspective it is desirable to use simple intermolecular potentials such as either SPC/E[8] or TIP4P/2005[15] because they are computationally easy to handle and included in many software packages.

The question that was left unanswered by previous work is can such simple intermolecular potentials also provide good predictions of thermodynamic properties? Addressing this issue is particularly important when studying mixtures in which water is a crucial component. For example, water is an important contributor to many biological systems. However, in the modeling of such systems, the main emphasis is often on the biomolecule or macromolecule and a simple representation of water is used. Indeed, the force fields of biomolecules are commonly parameterized for particular water potentials. Therefore, information regarding the limitations of water potentials is also highly desirable for improving the prediction of aqueous mixtures.

The goal of this work is to address this issue by calculating the thermodynamic properties of water from ambient conditions to the critical temperature using the SPC/E and TIP4P/2005 potentials and comparing the results to both experimental data and results obtained from the MCYna potential. This comparison will allow us to further elucidate the influence of polarization on the prediction of the thermodynamic properties of water.

II. MOLECULAR SIMULATION

A. Brief overview of the method

The method used for the *NVT* ensemble is based on the Massieu-Planck[24] system of thermodynamics and proceeds from the fundamental entropy equation $S(N, V, E)$ and devises different forms, such as the Helmholtz function $A/T = A(N, V, 1/T)$, via successive Legendre transformations.[24] Lustig[17] extensively described details of the *NVT* ensemble formalism and only the salient features are given here. In statistical mechanics the Helmholtz function A/T is connected with the logarithm of the partition function $\Pi(\beta, V, N)$ via the simple relationship

$$-\beta A(\beta, V, N) = \ln \Pi(\beta, V, N), \tag{1}$$

where $\beta = 1/kT$ and k is Boltzmann's constant. As a consequence, any thermodynamic property can be obtained from some combination of partial derivatives of the function $A(N, V, 1/T)$, or equivalently of the function $\Pi(\beta, V, N)$. The basic partial derivative of the partition function $\Pi(\beta, V, N)$ with respect to the independent state variables β and V has the following form:

$$\Pi_{mn} = \frac{1}{\Pi}\frac{\partial^{m+n}\Pi}{\partial\beta^m \partial V^n}. \tag{2}$$

The general expression of Π_{mn} can be identified with the ensemble averages of configurational properties

$$\Pi_{mn} = \left(\frac{F/2}{-\beta}\right)^m \left(\frac{N}{V}\right)^n \left(\mathrm{P}_{0,n}^{-N} \sum_{j=0}^{m} \binom{m}{j} \mathrm{P}_{0,m-j}^{-F/2} \left\langle \left[\frac{\beta U(q)}{F/2}\right]^j \right\rangle_{NVT} + (1-\delta_{0n}) \sum_{j=0}^{m} \binom{m}{j} \sum_{i=1}^{n} \binom{n}{i} \mathrm{P}_{0,n-i}^{-N} \sum_{l=1}^{i} \mathrm{P}_{-l,m-j}^{F/2} \frac{1}{N^{i-l}} \times \left\langle \left[\frac{\beta U(q)}{F/2}\right]^j \sum_{k=1}^{k_{\max}(i,l)} c_{ilk} \frac{V^i W_{ilk}}{N^l} \right\rangle_{NVT} \right), \tag{3}$$

where $\langle ... \rangle$ is the *NVT* ensemble average and δ_{ij} is the Kronecker delta. The $\mathrm{P}_{l,m}^{k}$ polynomial and the term $c_{ilk}W_{ilk}$ which is a product of negative volume derivatives $W_{ilk} = -(\partial^i \beta U/\partial V^i)_{\beta,N}$ of the potential energy divided by temperature are described in detail in Ref. 17.

The formalism outlined above is valid for any assumed intermolecular potential energy function $U(\mathbf{q})$. In this work we restrict ourselves to molecular pair interaction of atomic systems $U(\mathbf{q}) = \sum_{i=1}^{N-1} \sum_{j=i+1}^{N} u_{ij}(r_{ij})$, where r_{ij} is the distance between atoms i and j. The volume derivatives of nth order are given by

$$\frac{\partial^n U}{\partial V^n} = \frac{1}{3^n V^n} \sum_{j=1}^{N-1} \sum_{j=i+1}^{N} \sum_{k=1}^{n} a_{nk} r_{ij}^k \frac{\partial^k u_{ij}}{\partial r_{ij}^k}, \tag{4}$$

where the coefficients a_{nk} are constructed using recursive relations.[17] All thermodynamic properties are then expressed in terms of *NVT* partition functions via Eqs. (2) and (4). The resulting thermodynamic state variables used in our study are summarized in Table I.

B. Intermolecular potentials

This work is focused on two of the most widely used rigid water models, namely, the SPC/E[8] and TIP4P/2005[15] potentials. These potentials are computationally efficient and provide a very good representation of many properties of liquid water at ambient conditions.[11] As such, they are an appropriate starting point for investigating liquid water over a wider range of temperature and pressure. In both cases, the potentials combine contributions from both Lennard-Jones

TABLE I. Thermodynamic properties expressed in terms of derivatives of the partition function.[17]

Thermal pressure coefficient	$\gamma_V = k\Pi_{01} - (\Pi_{11} - \Pi_{01}\Pi_{10})/T$
Isothermal compressibility	$\frac{1}{\beta_T} = -VkT(\Pi_{02} - \Pi_{01}^2)$
Adiabatic compressibility	$\frac{1}{\beta_S} = \frac{1}{\beta_T} + \frac{TV}{N}\frac{\gamma_V^2}{C_V}$
Thermal expansion coefficient	$\alpha_p = \gamma_V \beta_T$
Isochoric heat capacity	$C_V = \frac{\Pi_{20} - \Pi_{10}^2}{NkT^2}$
Isobaric heat capacity	$C_P = C_V - \frac{k\Pi_{01} - (\Pi_{11} - \Pi_{01}\Pi_{10})^2/T}{N(\Pi_{02} - \Pi_{01}^2)}$
Speed of sound	$\omega_0^2 = \frac{V}{M\beta_S}$
Joule-Thomson coefficient[a]	$\mu_{JT} = \frac{\gamma_V - 1/(T\beta_T)}{N \cdot C_V/(VT\beta_T) + \gamma_V^2}$

[a]Note that in Ref. 17, the sign in the numerator of Eq. (20c) is reversed.

interactions and an electrostatic term:

$$u(\vec{r}) = 4\varepsilon \sum_{i}^{N} \sum_{j \neq i}^{N} \left\{ \left(\frac{\sigma}{r_{ij}^{oo}} \right)^{12} - \left(\frac{\sigma}{r_{ij}^{oo}} \right)^{6} \right\} + \frac{1}{4\pi\varepsilon_0} \sum_{i}^{N} \sum_{j \neq i}^{N} \frac{q_i q_j}{r_{ij}}, \quad (5)$$

where r_{ij} and r_{ij}^{oo} are the distances between charged sites and oxygen atoms, respectively, and ε_0 is the permittivity of the vacuum. The SPC/E and TIP4P/2005 models differ with respect to the geometry of the water molecule and the values of the size (σ) and energy (ε) parameters, and charges q_i.

The SPC/E potential uses a rigid three-site water model with an oxygen-hydrogen (O–H) distance of 1 Å and a H–O–H angle of 109.47°. Values of the parameters are $\sigma = 3.166$ Å and $\varepsilon = 0.65$ kJ/mol with a charge of +0.4238 on both H atoms and a charge of −0.8427 on the O atom. The TIP4P/2005 potential uses a rigid four-site water model with an O–H distance of 0.9572 Å and a H–O–H angle of 104.52°. Values of the parameters are $\sigma = 3.1589$ Å and $\varepsilon = 0.7749$ kJ/mol with a charge of +0.5564 on both H atoms. A significant difference for the TIP4P/2005 potential compared to the SPC/E potential is a charge of −1.1128 that is not located on the O atom but is instead displaced by 0.1546 Å on a bisector between the H atoms.

The equilibrium and coexistence properties of these two models have been extensively investigated.[8,11,13] Vega and Abascal[11] reported a detailed comparison of the accuracy of popular rigid and non-polarizable water models. The main conclusion from this analysis was that the SPC/E and TIP4P/2005 are the most accurate three-site and four-site models, respectively. The TIP4P/2005 and SPC/E potentials were developed to fit properties such as the temperature of maximum density, vapor-liquid equilibria, and enthalpy of vaporisation of liquid water at ambient conditions. The TIP4P/2005 potential can be also used to correctly reproduce the water-ice phase diagram. However, these potentials also have a number of shortcomings such as: a low temperature of maximum density; a high expansion coefficient (SPC/E); low dielectric constants (TIP4P/2005); and a low dipole moment (SPC/E and TIP4P/2005). These deficiencies can be at least partly attributed to the nature of the parameterization, which was targeted at optimizing agreement with other properties.

Polarizability is being increasingly recognised as an important contribution for improving the predictive capability of water intermolecular potentials. As reviewed in Ref. 25, more than 20 polarizable water models have been developed with varying success, e.g., MCY,[23] SPC flexible charge,[26] (SPCFQ), revised polarization[27] (RPOL), and the Gaussian charge polarizable model[28] (GCPM) potentials. Some early polarizable models proved to be inferior to their non-polarizable counterparts,[25] which can be partly explained by limitations of computational resources. However, more recently good results[21,29–31] have been reported for polarizable potentials such as the MCYna[21] and Baranyai-Kiss[29] (BKd3) potentials.

The MCYna intermolecular potential is the sum of two-body additive u_2, non-additive three-body u_3, and polarizable u^{pol} contributions

$$u(\vec{r}) = \sum_{i<j}^{N} u_2(\vec{r}_i, \vec{r}_j) + \sum_{i<j<k}^{N} u_3(\vec{r}_i, \vec{r}_j, \vec{r}_j) + u^{pol}. \quad (6)$$

The contribution of two-body interactions is obtained from the *ab initio* MCY potential:[20]

$$\begin{aligned} u_2 = {} & q^2 \cdot \left(\frac{1}{r_{13}} + \frac{1}{r_{14}} + \frac{1}{r_{23}} + \frac{1}{r_{24}} \right) + \frac{4q^2}{r_{78}} \\ & - 2q^2 \left(\frac{1}{r_{18}} + \frac{1}{r_{28}} + \frac{1}{r_{37}} + \frac{1}{r_{47}} \right) + a_1 e^{(-b_1 r_{56})} \\ & + a_2 (e^{(-b_2 r_{13})} + e^{(-b_2 r_{14})} + e^{(-b_2 r_{23})} + e^{(-b_2 r_{24})}) \\ & + a_3 (e^{(-b_3 r_{16})} + e^{(-b_3 r_{26})} + e^{(-b_3 r_{35})} + e^{(-b_3 r_{45})}) \\ & - a_4 (e^{(-b_4 r_{16})} + e^{(-b_4 r_{26})} + e^{(-b_4 r_{35})} + e^{(-b_4 r_{45})}). \end{aligned} \quad (7)$$

The meaning of the parameters is the same as given in the literature.[22,23] The non-additive contributions to intermolecular interactions arise for induction interactions, resulting from molecular polarizability, short-range repulsion, and dispersion interactions. The MCYna potential uses the Axilrod-Teller[32] triple dipole term to account for non-additive dispersion interactions,

$$u_3 = \frac{\nu(1 + 3\cos\theta_i \cos\theta_j \cos\theta_k)}{(r_{ij} r_{ik} r_{jk})^3}, \quad (8)$$

where θ_i, θ_j, and θ_k are inside angles of the triangle formed by three atoms denoted by i, j, and k, and r_{ij}, r_{ik}, and r_{jk} are the three side lengths of the triangle. The parameter ν is the non-additive coefficient, which can be determined from experiment. The value of u^{pol} is obtained by determining the contribution of induced dipoles as detailed in Ref. 22. The polarisation term is defined as

$$u^{pol} = -\frac{1}{2} \sum_{i=1}^{N} \vec{\mu}_i^{\,\mathrm{int}} \cdot \vec{E}_i^{\,o}, \quad (9)$$

where $\vec{E}_0$ is the electrostatic field of surrounding charges, and $\vec{\mu}_i^{\,\mathrm{int}}$ is the induced dipole at site i given by

$$\vec{\mu}_i^{ind} = \alpha\beta \cdot \vec{E}_i = \alpha\beta \cdot \left[\vec{E}_i^{\,o} + \sum_{j=1, j\neq i}^{N} T_{ij} \vec{\mu}_j^{ind} \right]. \quad (10)$$

In Eq. (10) $\alpha\beta$ is the polarizability and T_{ij} is the dipole tensor given by

$$T_{ij} = \frac{1}{4\pi\varepsilon_o r_{ij}^5} \left[3 r_{ij} r'_{ij} - r_{ij}^2 \right]. \quad (11)$$

Molecular systems are generally characterised by charge conservation, which means that only monopole and dipole terms (the first and the second terms inside the square brackets in Eq. (10)) are necessary. To simplify the calculation, intramolecular interactions are not considered. This means that the induced dipole has no interaction with the partial charges on the same water molecule. As discussed in Ref. 22, to improve the calculation of the induced dipole, the polarizability coefficient $\alpha = 1.44$ Å^3 is scaled by a factor of $\beta = 0.557503$ yielding in a polarizability term of $\alpha\beta = 0.802804$ Å^3. This

results in a dipole moment of 2.9 D, with 0.9 D attributed to induction interactions. The u^{pol} term is the dominant non-additive contribution, typically accounting for 30% of the total energy. In comparison u_3 contributes approximately 1%–2% to the total energy.[22]

C. Simulation details

Canonical *NVT* molecular dynamics simulations using the Shake algorithm[3] were performed for systems of $N = 500$ water molecules with a density of 0.998 g/cm^3 and a temperature range of 278–650 K. The Ewald summation method was used to evaluate the long-range part of the Coulomb potential.[3] The convergence parameter for the Ewald sum was $\alpha = 5.0/L$, with summation over $5 \times 5 \times 5$ reciprocal lattice vectors, where L is the box length. A cut-off of $L/2$ was applied to two-body interactions. During the pre-equilibration stage, the temperature was held constant by rescaling the velocities every ten steps, which we found to be equivalent to results obtained using a Gaussian thermostat. The simulations were commenced from an initial face centered cubic lattice with a time step of 2 fs. The systems were equilibrated for 500 ps before any ensemble averages were determined. At each temperature, the total simulation time was at least 2 ns, which corresponds to 10^6 time steps. The equations of motion were integrated using a leap-frog algorithm.[3] Ensemble averages were obtained by analysing post-equilibrium configurations at intervals of 100 time steps and standard deviations were determined. The calculated standard errors for many quantities illustrated in Figs. 1–9 are similar to the size of the symbols and error bars have been omitted.

III. RESULTS AND DISCUSSION

A. Reference data for water

Most of the experimental data for water reported in the literature[2] are at isobaric conditions whereas the MD simulations in the *NVT* ensemble[3] yield isochoric values.

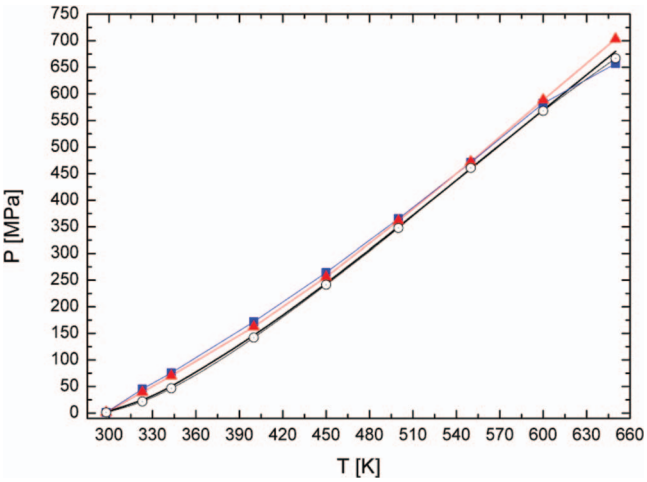

FIG. 1. Pressure-temperature behavior of liquid water at a constant density of 0.998 g/cm^3 predicted by the SPC/E (blue ■), TIP4P/2005 (red ▲), and MCYna potential[21] (○) and compared to experimental data[33] for water (—). The lines through the data points are given only for guidance.

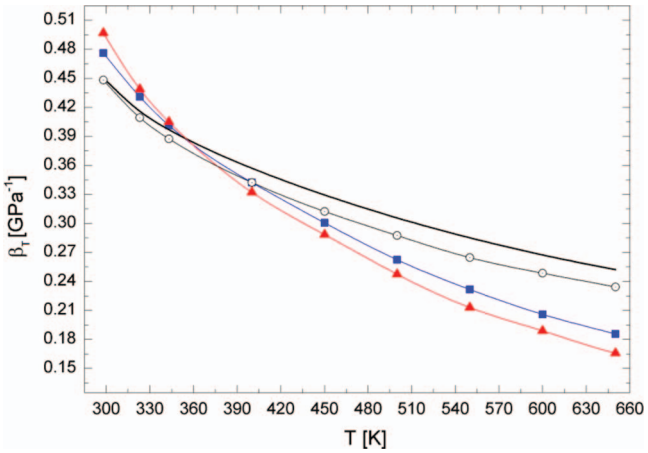

FIG. 2. Isothermal compressibility as a function of temperature predicted by the SPC/E (blue ■), TIP4P/2005 (red ▲), and MCYna potential[21] (○) and compared to experimental data[33] for water (—). The lines through the data points are given only for guidance.

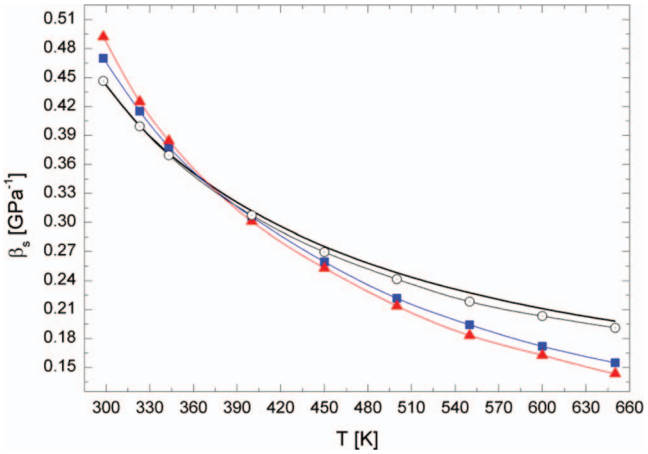

FIG. 3. Adiabatic compressibility as a function of temperature predicted by the SPC/E (blue ■), TIP4P/2005 (red ▲), and MCYna potential[21] (○) and compared to experimental data[33] for water (—). The lines through the data points are given only for guidance.

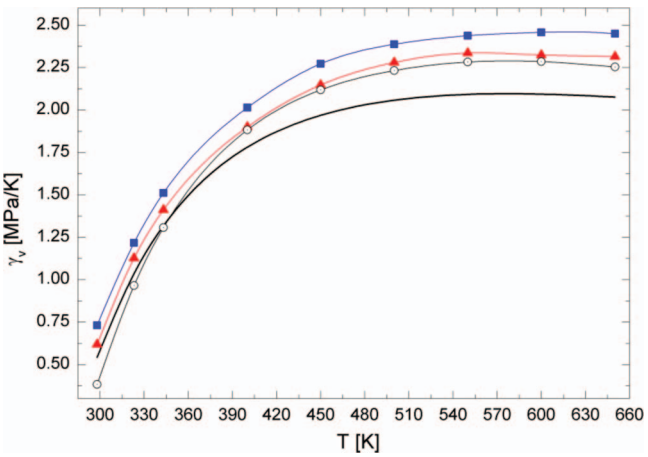

FIG. 4. Thermal pressure coefficient as a function of temperature predicted by the SPC/E (blue ■), TIP4P/2005 (red ▲), and MCYna potential[21] (○) and compared to experimental data[33] for water (—). The lines through the data points are given only for guidance.

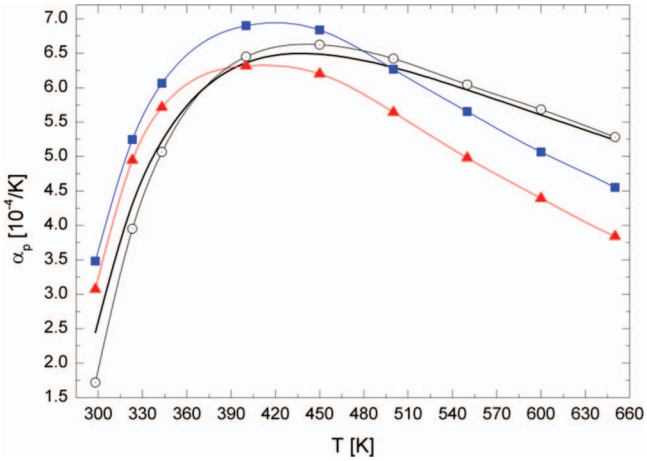

FIG. 5. Thermal expansion coefficient as a function of temperature predicted by the SPC/E (blue ■), TIP4P/2005 (red ▲), and MCYna potential[21] (○) and compared to experimental data[33] for water (—). The lines through the data points are given only for guidance.

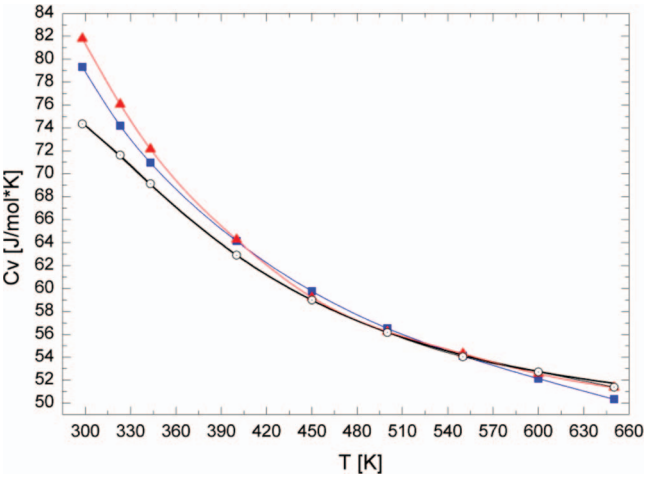

FIG. 6. Isochoric heat capacity as a function of temperature predicted by the SPC/E (blue ■), TIP4P/2005 (red ▲), and MCYna potential[21] (○) and compared to experimental data[33] for water (—). The lines through the data points are given only for guidance.

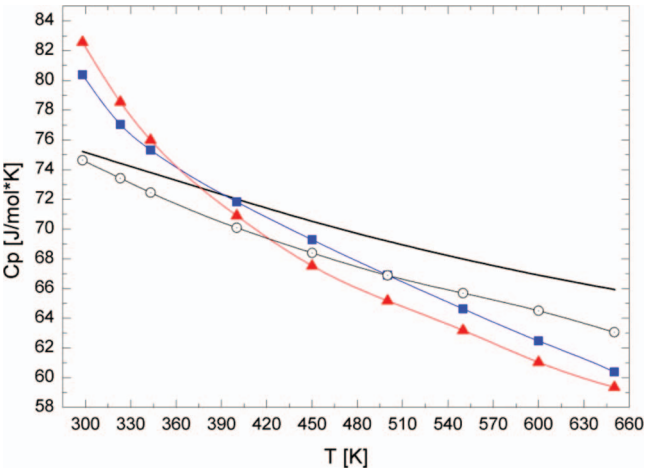

FIG. 7. Isobaric heat capacity as a function of temperature predicted by the SPC/E (blue ■), TIP4P/2005 (red ▲), and MCYna potential[21] (○) and compared to experimental data[33] for water (—). The lines through the data points are given only for guidance.

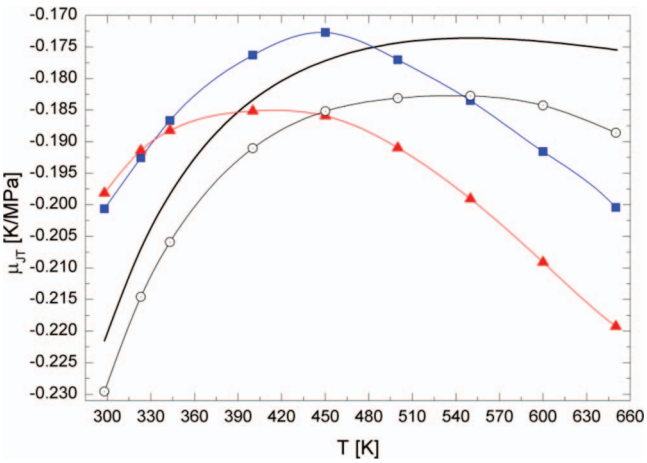

FIG. 8. Joule-Thomson coefficient as a function of temperature predicted by the SPC/E (blue ■), TIP4P/2005 (red ▲), and MCYna potential[21] (○) and compared to experimental data[33] for water (—). The lines through the data points are given only for guidance.

Therefore, we must either convert the data or find an accurate alternative to the experimental values. For this purpose, we have used the International Association for the Properties of Water and Steam (IAPWS-95) software developed by Wagner[33] to calculate thermodynamic quantities at isochoric conditions. However, IAPWS-95 can only be used to directly calculate p, C_V, C_P, μ_{JT}, and w_0. The remaining thermodynamic quantities, namely, β_T, β_S, γ_V, and α_P are then calculated using the following well-known relationships:[24]

$$\left.\begin{aligned} \beta_S &= \frac{V}{w_0^2 M} \\ \beta_T &= \frac{\beta_S C_P}{C_V} \\ \gamma_V^2 &= \frac{C_V\left(\beta_S^{-1}-\beta_T^{-1}\right)}{TV} \\ \alpha_P &= \frac{\mu_{JT} C_P}{TV} + \frac{1}{T} \end{aligned}\right\}, \tag{12}$$

where M is the total mass of the system.

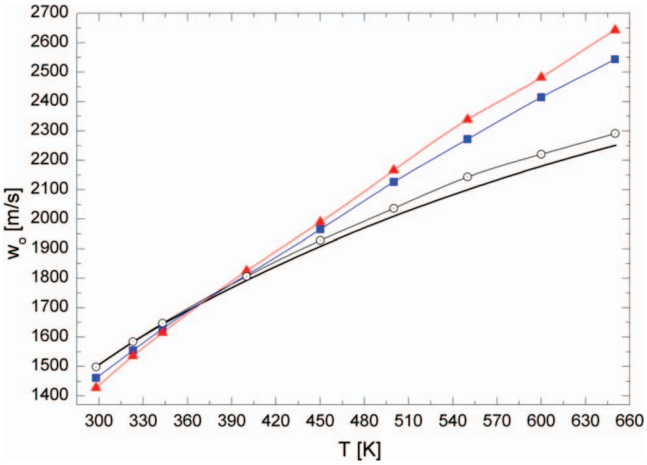

FIG. 9. Speed of sound as a function of temperature predicted by the SPC/E (blue ■), TIP4P/2005 (red ▲), and MCYna potential[21] (○) and compared to experimental data[33] for water (—). The lines through the data points are given only for guidance.

TABLE II. Comparison with experiment for the thermodynamic properties of several water potentials at 298 K and 0.1 MPa.

Potential	C_V (J/mol K)	C_P (J/mol K)	β_T (1/GPa)	β_S (1/GPa)	γ_V (MPa/K)	α_P (10^{-4}/K)	μ_{JT} (K/MPa)	w_0 (m/s)	Ref.
SPC	62.350	76.674	0.461	0.375[a]	1.629[a]	7.51	−0.2034[a]	1635.7[a]	10, 34
SPC/E	79.325	80.385	0.476	0.470	0.731	3.48	−0.2006	1460.1	This work
SPC/Fw	…	114.592	0.458	…	1.107[a]	2.00	…	…	10
TIP4P	82.089	88.975	0.590	0.544[a]	0.746[a]	4.4	−0.1872[a]	1357.4[a]	14, 34
TIP4P/2005	81.797	82.582	0.497	0.492	0.618[a]	3.08	−0.1937	1427.2	This work
TIP5P	118.239	90.587	0.410	0.535[a]	1.177[a]	6.30	−0.1275[a]	1369.0[a]	14, 34
GCPM	…	94.0	…	…	…	4.20	…	…	28
MCY	70.800	…	…	…	…	…	…	3040.0	23, 47
MCYna	74.357	74.636	0.448	0.446	0.383	2.63	−0.2295	1498.4	21
BKd3	…	88.0	0.450	…	0.488[a]	2.20	…	…	29
IAPWS-95	74.836	75.770	0.448	0.446	0.567	2.54	−0.2215	1499.7	33
Experiment	**74.44**	**75.312**	**0.458**	**0.425**	**0.436**	**2.00**	**−0.2216**	**1496.7**	2

[a]These values were calculated in this work from properties reported in the literature using the standard thermodynamic relationships given in Eq. (12).

B. Ambient thermodynamic properties

Table II compares experimental and simulation data for a range of thermodynamic properties obtained from various popular water models at 298 K and 0.1 MPa. The large range in the values highlights the different abilities of the models to correctly predict thermodynamic properties of water, and the absence of one all-purpose water potential. To some extent, this disparity can be attributed to different force-field implementations and calculation techniques. Comparative studies performed by Mao and Zhang,[34] Wu *et al.*,[10] and Vega and Abascal,[4] unexpectedly showed different results for the same water model. For example, different values were obtained for the isochoric and isobaric heat capacities using the Ewald[3] and particle-particle particle-mesh[3] (PPPM) methods. The unified calculation approach used here should reduce the discrepancies between values obtained for the various thermodynamic properties.

C. Pressure

The temperature-pressure behavior of water in the liquid phase is shown in Fig. 1. The IAPWS-95 reference data increases nonlinearly up to the normal boiling temperature, at which point the data increases almost linearly. The initial trend is probably caused by a reorganisation of the water structure, namely, a gradual retreat from classical tetrahedral structure, and increasing thermal fluctuations of the H-bond network.

Both the SPC/E and TIP4P/2005 potentials show good agreement with the IAPWS-95 data.[33] Simulated pressures from both water potentials show a close to a linear trend for the whole range of temperatures. These potentials slightly overestimate experimental data for the entire temperature range. From 298 K and up to 420 K the discrepancy is slightly higher which may be due to the excessive rigidity of the non-polarizable SPC/E and TIP4P/2005 models. In contrast, the isochore calculated from the MCYna potential[21] is in much better agreement with the experimental data over the entire range of temperatures and it accurately reproduces the non-linear behavior of pressure at low temperatures.

D. Isothermal and adiabatic compressibilities

The isothermal and adiabatic compressibilities reflect how the density of the system changes with pressure. Compressibility has a complex dependence from the local density of water and water clusters and the strength of hydrogen bonding. Both isothermal and adiabatic compressibilities at ambient conditions have a value of 0.45 GPa^{-1}, which is strongly influenced by the cohesive nature of extensive H-bonding. Due to strong thermal fluctuations with increasing temperature, the structure of water starts collapsing, opening up large cavities inside the H-bond network, and resulting in a more open structure. As a consequence of this structural change, the compressibility of water decreases with increasing temperature and pressure.

Simulation results for β_T and β_S as functions of temperature are compared with experimental data in Figs. 2 and 3, respectively. The SPC/E and TIP4P/2005 potentials at 298 K have values of $\beta_T = 0.476$ and 0.497 GPa^{-1}, respectively, which is consistent with previous calculations.[8,10,11] As reported by Wu *et al.*[10] and Abascal and Vega[11] most rigid potentials of the SPC and TIP families have thermal compressibilities higher than that of real water. In contrast, flexible SPC/Fw and F3C models have smaller β_T, which indicate the influence of internal degrees of freedom.[10]

Unlike constant pressure values,[35] β_T and β_S at a constant density of 0.998 g/cm^3 keep gradually decreasing and do not show any minima. At temperatures up to the normal boiling temperature, the isothermal and adiabatic compressibilities predicted by both the SPC/E and TIP4P/2005 potentials are overestimated. Data from these potentials gradually decrease with temperature, levelling off with the experimental data at around 355 and 373 K for β_T and β_S, respectively. After 373 K, the calculated curves for both figures keep descending below the experimental data.

Data obtained recently for the MCYna potential[21] are also illustrated in Figs. 2 and 3. The comparison shows that the MCYna results are in much better agreement with the experimental curve for both β_T and β_S. The underestimation of β_T and β_S of water for the non-polarizable SPC/E and TIP4P/2005 potentials and, to a much smaller extent, the

MCYna potential can be attributed to inadequate temperature dependence of the water structure at high temperatures provided by these potentials. As was shown recently[30,31] non-polarizable potentials from the SPC-family underestimate the level of water structure at temperatures approaching the critical temperature, particularly number of hydrogen bonds.

It is well known[36] that water at critical conditions maintains a much more stable shell structure and higher level of H-bonding then predicted by any potential model. Svischev and Kusalik,[37] and Shiga and Shinoda[38] identified a specific feature of SPC based models that could be responsible for underestimating H-bonded configurations. The rotational self-diffusion coefficient[37] in the H-bonding plane for the SPC/E potential is half the value observed for other planes. That is, the angle between the intra-molecular H–O covalent bond and intermolecular O···O vector (H–O···O) for the H-bonded pair can occur within a narrow range of values. Path integral molecular dynamics (PIMD) simulations have revealed[38] that the quantum corrections significantly broaden the H–O···O angle distribution in both liquid and solid phases, allowing for better H-bonding.

Although quantum correction calculations remain computationally and theoretically challenging, accounting for polarisation interactions or bond vibrations can improve predictions of the density dependent properties such as compressibilities, thermal expansion, and thermal pressure coefficients for a wide range of state points. Recent simulation studies[30,31] using the MCYna potential, which takes into account non-additive effects like polarization, have reported an improved description of the H-bond network and shell structure even at high temperatures.

E. Thermal pressure coefficient

The thermal pressure coefficient is defined as the differential dependence of pressure on temperature of a system perturbed by a change in temperature where the volume remains constant. It is closely related to various properties such as internal pressure, speed of sound, the entropy of melting, isothermal compressibility, isobaric expansibility, etc.

The thermal pressure coefficient as a function of temperature is illustrated in Fig. 4. γ_V values for the SPC/E and TIP4P/2005 potentials start from 0.731 and 0.618 MPa/K, respectively, and increase almost linearly until the boiling temperature. Thereafter, γ_V starts slowing down, peaking at around 550–580 K with a further tendency to decrease. Both the SPC/E and TIP4P/2005 potentials give higher values of γ_V than the experimental data throughout the whole temperature range. The results for the TIP4P/2005 potential are in slightly better agreement with experiment than the SPC/E data. Our observations are consistent with results reported in the reviews of Wu *et al.*[10] and Vega and Abascal.[11] All non-polarizable water models vastly overestimate the pressure coefficient at 298 K. Over estimation of the experimental value $\gamma_V = 0.436$ MPa/K by some 30%–200% strongly indicates that all non-polarizable water models reported in Refs. 4 and 6 fail to describe the temperature dependence of pressure at ambient conditions.

It is apparent from the comparison given in Fig. 4 and Table II that the MCYna potential yields the closest agreement with the experimental data. This may reflect the better description of interatomic interactions given by the MCYna potential, namely, the contributions from non-additive terms. Experimentally, the thermal pressure coefficient becomes negative at temperatures less than 277 K with anomalous density behavior.[35] Positive values of the thermal pressure coefficient at all temperatures studied implies that water does not show anomalies at a density of 0.998 g/cm^3.

F. Thermal expansion coefficient

The thermal expansion coefficient is a measure of the tendency of matter to change volume in response to a change in temperature. While anomalous volume behavior of water and ice in the temperature region from −4 until +4 °C is well known, the present data provide information about the temperature dependence of α_P at constant volume. Simulation results for α_P are compared with experimental data for water in Fig. 5. Unlike constant pressure data,[2] values of α_P at constant volume increase more slowly, starting to slow down after 350 K and eventually peaking at around 425–450 K. The initial increase in α_P can be attributed to the temperature driven collapse of water structure rather than lowering of water density. Thereafter, the decrease in thermal expansion coefficient is caused by the constraint imposed on the system's volume.

Values of α_P calculated from the method described in this work at 298 K for SPC/E (3.482×10^{-4}/K) and TIP4P/2005 (3.076×10^{-4}/K) models are in much better agreement with the experimental value $2.56\ 10^{-4}$/K than most of the water models reported in Refs. 10 and 15. For example, the value of α_P for the SPC/E potential obtained from the fluctuation formula is 5.14×10^{-4}/K. In the temperature range of 298–425 K, the thermal expansion coefficients obtained using the SPC/E and TIP4P/2005 potentials overestimate the experimental data. Peaking at around 425 K both curves start to decrease, significantly deviating from the experimental data. It is apparent that MCYna potential most closely mimics the behavior of the IAPWS-95 curve.

The temperature trend is caused by the interplay between isothermal compressibility β_T and pressure coefficient γ_V (see Table I). According to the classical fluctuation formula,[15] β_T is proportional to volume fluctuations. As can be seen from Figs. 3 and 4, the density constraint means that, shortly after the normal boiling temperature, local volume fluctuations decrease with temperature and outweigh the increase in pressure. This temperature dependence of local volume fluctuations is a characteristic of the NVT ensemble and plays important role in other density dependent properties, such as the Joule-Thomson coefficient and speed of sound.

G. Isochoric and isobaric heat capacities

The isochoric and isobaric heat capacities of water as a function of temperature from our simulations and experimental data are illustrated in Figs. 6 and 7, respectively. The curves from both water models decrease progressively with

increasing temperature, following each other rather closely. The TIP4P/2005 potential gives slightly higher values of C_V and C_P than the SPC/E curve at ambient conditions and slightly lower at high temperatures. The behavior of the C_P curve is especially interesting because it does not show any minimum. The presence of a shallow C_P minimum at around 309 K and subsequent increase with temperature, at constant pressure conditions,[2] is caused by rearrangement in water clustering and the consequent increase of enthalpy. However, at constant volume, the values of C_P gradually decrease for the whole temperature range. At high pressures and temperatures the water structure apparently keeps deteriorating and the enthalpy decreases.

While agreement with IAPWS-95 data is quite good for isochoric heat capacity, with the exception of too high values at 298 K, the isobaric heat capacity curve deviates from the experimental data much more. As is evident from the relationships in Table I, the isobaric heat capacity is derived from the values of isochoric heat capacity and compressibilities. Therefore, an error in either of these thermodynamic quantities will be reflected in the results for the isobaric heat capacity. Extensive data for other potentials at different temperatures are not available in the literature. As can be seen from the comparison in Table II and the recent review by Mao and Zhang,[34] all non-polarizable potentials over-predict values of C_V and C_P at 298 K and 0.1 MPa, by at least 7%. This inadequacy has been observed for quite some time and it has not been rectified by the development of new rigid or flexible water models.

It is sometimes suggested that the over-prediction of C_P is caused by a failure to address quantum influences,[38,39] bond vibrations,[10] and polarization effects. Shiga and Shinoda[38] performed extensive PIMD calculations of vapor, liquid, and ice using a flexible SPC/F water model.[40] The C_V of ice and vapor was accurately reproduced whereas C_V for liquid water was 23% smaller than the experimental value 74.44 J/mol K. Nonetheless, this is a significant improvement over the classical SPC/F value of 116.395 J/mol K. Vega *et al.*[39] used a quantum corrected version of the TIP4P/2005 potential and obtained a value of C_P that was approximately only 5.8% less than the experimental value 75.312 J/mol K. Shiga and Shinoda[38] observed that success in predicting C_V for vapor and ice indicates that the vibrational heat capacity is predicted correctly, whereas underestimation in liquid phase means an inadequate description of hydrogen-bonded configurations.

Accounting for polarisation effects is a viable alternative to costly PIMD simulations because the classical treatment of intermolecular bond vibrations causes significant overestimation of heat capacity.[10,40] Abascal and Vega[15] showed that including the self-energy correction[8] helps to bring values of heat capacity C_P and heat of vaporisation (ΔH_v) significantly closer to experimental values by reducing non-corrected values of C_P and ΔH_v by more than 11% each. However, the self-energy correction $\Delta E_{pol} = (\vec{\mu}_l - \vec{\mu}_g)^2/2\alpha$ for the SPC/E and TIP4P/2005 is constant because the liquid and the gas phase dipole moments of these models are constant. Increasing deviations of C_V and C_P in the high temperature region on Figs. 5 and 6 indicates that constant ΔE_{pol} alone cannot improve heat capacity predictions in the wide temperature range.

Heat capacities obtained from the MCYna water potential, which explicitly accounts for polarization interaction via induced dipole moment (see Eqs. (9)–(11)) are also presented in Figs. 6 and 7. The MCYna potential gives remarkably good agreement of C_V values with IAPWS-95 data, while C_P values underestimate the experimental data throughout the whole temperature range. It is apparent from the comparison of the isobaric heat capacities (Figs. 6 and 7) that the MCYna potential yields the best agreement with experiment. The superiority of the polarizable MCYna results over nonpolarizable SPC/E and TIP4P/2005 results clearly demonstrates the importance of polarization as a key-contributing factor. The MCYna calculations did not need to invoke quantum corrections to obtain good agreement with experiment.

H. Joule-Thomson coefficient

Joule-Thomson expansion,[17,18,41] or throttling of a fluid of constant composition is a closed-system process occurring between initial and final states at pressures p_0 and p_1, with $p_0 > p_1$, for which the system enthalpy remains constant. The sign of the Joule-Thomson coefficient μ_{JT} at any given state determines whether the fluid is cooled ($\mu_{JT} > 0$) or heated ($\mu_{JT} < 0$) for a small change in pressure at constant enthalpy. Joule-Thomson heating of water is of particular interest in industry because it has a significant influence on temperature in and around injection wells.

The simulation results are compared with experimental data in Fig. 8. The Joule-Thomson coefficient is negative for the entire simulation region, which naturally indicates heating of water at increased pressures. All three potentials fail to reproduce temperature dependence of μ_{JT}. Both the TIP4P/2005 and SPC/E potentials give too high values of μ_{JT} at temperatures up to 420–500 K. After this temperature region, results from both non-polarizable potentials start to decrease almost linearly. Only the MCYna potential qualitatively reproduces the behavior of the experimental data at all temperatures, although the value of the Joule-Thomson coefficient is under-predicted. The disparity increases with increasing temperature. Using well-known thermodynamic relationships[24] we can rewrite the formula for μ_{JT} from Table I in the following form $\mu_{JT} = \frac{V}{C_P}(\alpha_P \cdot T - 1)$ and it is immediately apparent that the observed temperature dependence of the Joule-Thomson coefficients is consistent with the trend observed for the thermal expansion coefficient (see Fig. 5).

I. Speed of sound

The speed of sound in water[42,43] as a function of temperature is illustrated in Fig. 9. The thermodynamic properties at constant volume behave quite differently than at constant pressure. Similar to many other thermodynamic properties, the speed of sound at isobaric conditions goes through a peak at around 348 K and than decreases with temperature.[2] At isochoric conditions compressibility does not have a minimum, and simply decreases with temperature. The thermodynamic speed of sound is related to the propagation of an adiabatic pressure wave. As can be seen from Table II, w_0 is inversely

proportional to the adiabatic compressibility, and therefore, keeps freely increasing with temperature and pressure.

Results from the TIP4P/2005 and SPC/E potentials shown in Fig. 9 are only in qualitative agreement with the experimental data. Starting from values at 298 K of 1420 m/s (TIP4P/2005) or 1460 m/s (SPC/E), the simulation results cross the experimental data at approximately 373 K. In both cases the predicted speed of sound increases linearly with temperature, almost doubling in value at 650 K. The speed of sound is inversely proportional to square root of density and adiabatic compressibility β_S of water (see Table I). While the overall density of a system remains constant, it is the adiabatic compressibility (see Fig. 3) that determines the temperature dependence speed of sound. The high values of w_0 could be attributed to specific structure and local density behavior of TIP4P/2005 and SPC/E models. It has been shown,[43] that over a range of high frequencies (>4 nm^{-1}) liquid water behaves as though it is a glassy solid rather than a liquid and sound travels at about twice its normal speed (~3200 m/s, similar to the speed of sound in ice Ih).

It is apparent from Fig. 9 that the MCYna potential yields the best agreement with the experimental data for temperatures up to 400 K. At higher temperatures the MCYna potential also over-predicts the speed of sound, however, to a much smaller extent than the non-polarizable potentials.

IV. CONCLUSIONS

Results for both the TIP4P/2005 and SPC/E potentials are only in qualitative agreement with experimental data for water. At temperatures greater than 400 K, the TIP4P/2005 and SPC/E potentials fail to accurately reproduce the thermodynamic properties of liquid water. This is consistent with other work,[10,11,34] that indicated that all non-polarizable water models give values of heat capacities, compressibilities, and thermal expansion coefficient are in poor agreement with experiment even at 298 K and 0.1 MPa. To the best of our knowledge, our values of the Joule-Thomson coefficient and the speed of sound of SPC/E and TIP4P/2005 potentials are the only available data.

It is difficult to unambiguously differentiate between the SPC/E and TIP4P/2005 for thermodynamic properties. Although both potentials fail at high temperatures, at temperatures up to 400 K both models reproduce the overall experimental trend, with the SPC/E results being slightly closer to the IAPWS-95 reference data.[33] Deviations observed in the high temperature and pressure region can be attributed to the following reasons. Non-polarizable potentials like TIP4P/2005 and SPC/E significantly underestimate the water structure and H-bond network at high temperatures. According to these models, at high temperatures, water has a very small 1st oxygen-hydrogen solvation shell and an almost vanished 2nd solvation shell. However, recent *in situ* x-ray diffraction experiments of Ikeda *et al.*[44] and Weck *et al.*[45] indicate much better conservation of water shell structures and H-bonding at extreme pressures and temperatures. Furthermore, the *ab initio* calculations of Kang *et al.*[46] indicate a conservation of 50% of H-bonds above 800 K. From a thermodynamic point of view, the deviation from the reference data of the speed of sound, thermal pressure, thermal expansion, and Joule-Thomson coefficients for all three potentials can be attributed to the inadequate prediction of $\partial p/\partial T$ and $\partial V/\partial p$. This reflects that the temperature dependence of H-bonding and spatial shell structure is inadequately predicted by the SPC/E and TIP4P/2005 potentials.

An important factor for improving MD results for polar liquids like water is the inclusion of interaction terms that better describe changes in physical conditions at variable temperature and pressure. Quantum corrections could potentially improve prediction of thermodynamic properties of water, however few calculations in this direction have been done so far.[38,39] Accounting for the self-energy correction could certainly improve calculations of heat capacity and vaporization enthalpy, however it remains limited to ambient or near ambient conditions.[8,15]

Vega and Abascal[11] suggested including polarizability to improve agreement with experiment and our analysis strongly supports this conclusion. Our comparison with the most recent simulation data[21] obtained from the polarizable MCYna potential indicates that very good agreement with experimental data over the entire liquid range of temperatures is possible when polarization effects are included. Indeed, in some cases, the effect of including polarization is to transform poor agreement with experiment to near perfect agreement. Significantly, this is achieved without any arbitrary optimization of theory with experimental data. The data clearly indicate that accounting for polarization is important for accurately predicting the thermodynamic properties of water.

ACKNOWLEDGMENTS

I.S. thanks Swinburne University of Technology for support through a postgraduate scholarship. We thank the National Computational Infrastructure (NCI) for an allocation of computing time.

APPENDIX: EVALUATION OF PARTITION FUNCTION DERIVATIVES Π_{mn}

Derivatives[17] for the right-hand side of Eq. (2) used to evaluate the thermodynamic quantities in Table II:

$$\Pi_{10} = \left(-\frac{\beta}{F/2}\right)^{-1}\left[1+\left\langle\frac{\beta U}{F/2}\right\rangle\right], \tag{A1}$$

$$\Pi_{20} = \left(-\frac{\beta}{F/2}\right)^{-2}\left[\left(1+\frac{1}{F/2}\right)+2\left\langle\frac{\beta U}{F/2}\right\rangle+\left\langle\left(\frac{\beta U}{F/2}\right)^2\right\rangle\right], \tag{A2}$$

$$\Pi_{01} = \frac{N}{V}+\left\langle-\frac{\partial\beta U}{\partial V}\right\rangle, \tag{A3}$$

$$\Pi_{02} = \left(\frac{N}{V}\right)^2\left(1-\frac{1}{N}\right)+2\frac{N}{V}\left\langle-\frac{\partial\beta U}{\partial V}\right\rangle + \left\langle-\frac{\partial^2\beta U}{\partial V^2}\right\rangle+\left\langle\left(-\frac{\partial\beta U}{\partial V}\right)^2\right\rangle, \tag{A4}$$

$$\Pi_{11} = \left(\frac{\beta}{F/2}\right)^{-1}\left[\frac{N}{V}\left(1+\left\langle -\frac{\beta U}{F/2}\right\rangle\right) + \left(1-\frac{1}{F/2}\right)\left\langle -\frac{\partial \beta U}{\partial V}\right\rangle + \left\langle \frac{\beta U}{F/2}\left(-\frac{\partial \beta U}{\partial V}\right)\right\rangle\right], \tag{A5}$$

where F is total number of degrees of freedom of the system of molecules and $\beta = 1/kT$.

[1] Y. Wei and R. J. Sadus, AIChE J. **46**, 169 (2000); N. G. Stetenskaja, R. J. Sadus, and E. U. Franck, J. Phys. Chem. **99**, 4273 (1995); A. E. Mather, R. J. Sadus, and E. U. Franck, J. Chem. Thermodyn. **25**, 771 (1993).
[2] W. Wagner and A. Pruß, J. Phys. Chem. Ref. Data **31**, 387 (2002).
[3] R. J. Sadus, *Molecular Simulation of Fluids: Theory, Algorithms and Object-Orientation* (Elsevier, Amsterdam, 1999); Mol. Phys. **87**, 979 (1996).
[4] C. Vega, J. L. F. Abascal, M. M. Conde, and J. L. Aragones, Faraday Discuss. **141**, 251 (2009).
[5] R. Bukowski, K. Szalewicz, G. Groenenboom, and A. van der Avoird, Science **315**, 1249 (2007).
[6] W. Jorgensen, J. Chandrasekhar, J. Madura, R. Impey, and M. Klein, J. Chem. Phys. **79**, 926 (1983).
[7] H. J. C. Berendsen, J. P. M. Postma, W. F. van Gunsteren, and J. Hermans, in *Intermolecular Forces*, edited by B. Pullman (Reidel, Dordrecht, 1981).
[8] H. Berendsen, J. Grigera, and T. Straatsma, J. Phys. Chem. **91**, 6269 (1987).
[9] G. Raabe and R. J. Sadus, J. Chem. Phys. **137**, 104512 (2012).
[10] Y. Wu, H. L. Tepper, and G. A. Voth, J. Chem. Phys. **124**, 024503 (2006).
[11] C. Vega and J. L. F. Abascal, Phys. Chem. Chem. Phys. **13**, 19663 (2011).
[12] G. Raabe and R. J. Sadus, J. Chem. Phys. **134**, 234501 (2011).
[13] H. Pi, J. Aragones, C. Vega, E. Noya, J. Abascal, M. Gonzalez, and C. McBride, Mol. Phys. **107**, 365 (2009).
[14] M. Chaplin, *Water Structure and Science* (London South Bank University, 2013), see http://www.lsbu.ac.uk/water/anmlies.html.
[15] J. L. F. Abascal and C. Vega, J. Chem. Phys. **123**, 234505 (2005).
[16] L. Báez and P. Clancy, J. Chem. Phys. **101**, 9837 (1994); L. Dang and B. Pettitt, J. Phys. Chem. **91**, 3349 (1987); M. Mahoney and W. Jorgensen, J. Chem. Phys. **112**, 8910 (2000); R. Impey, P. Madden, and I. McDonald, Mol. Phys. **46**, 513 (1982); G. Lie and E. Clementi, Phys. Rev. A **33**, 2679 (1986); F. Stillinger and A. Rahman, J. Chem. Phys. **60**, 1545 (1974); H. Nada and J. M. van der Eerden, *ibid.* **118**, 7401 (2003); A. Soper and M. Phillips, Chem. Phys. **107**, 47 (1986).
[17] R. Lustig, Mol. Simul. **37**, 457 (2011); Mol. Phys. **110**, 3041 (2012).
[18] M. Li and W. L. Johnson, Phys. Rev. B **46**, 5237 (1992).
[19] L. I. Kioupis and E. J. Maginn, Fluid Phase Equilib. **200**, 75 (2002).
[20] R. Lustig, J. Chem. Phys. **100**, 3048 (1994); **100**, 3060 (1994); **100**, 3068 (1994); **109**, 8816 (1998).
[21] T. M. Yigzawe and R. J. Sadus, J. Chem. Phys. **138**, 044503 (2013).
[22] J. Li, Z. Zhou, and R. J. Sadus, J. Chem. Phys. **127**, 154509 (2007); Comput. Phys. Commun. **178**, 384 (2008).
[23] O. Matsuoka, E. Clementi, and M. Yoshimine, J. Chem. Phys. **64**, 1351 (1976).
[24] A. Münster, *Classical Thermodynamics*, translated by E. S. Halberstadt (Wiley, London, 1970).
[25] B. Guillot, J. Mol. Liq. **101**, 219 (2002).
[26] S. W. Rick, S. J. Stuart, and B. J. Berne, J. Chem. Phys. **101**, 6141 (1994).
[27] L. X. Dang, J. Chem. Phys. **97**, 2659 (1992).
[28] A. A. Chialvo and P. T. Cummings, Fluid Phase Equilib. **150–151**, 73 (1998); P. Paricaud, M. Predota, A. A. Chialvo, and P. T. Cummings, J. Chem. Phys. **122**, 244511 (2005).
[29] P. T. Kiss and A. Baranyai, J. Chem. Phys. **138**, 204507 (2013).
[30] I. Shvab and R. J. Sadus, Phys. Rev. E **85**, 051509 (2012).
[31] I. Shvab and R. J. Sadus, J. Chem. Phys. **137**, 124501 (2012).
[32] B. M. Axilrod and E. Teller, J. Chem. Phys. **11**, 299 (1943).
[33] W. Wagner, IAPWS-95 software was used to obtain reference data for water, see http://www.thermo.rub.de/en/prof-w-wagner/software/iapws-95.html.
[34] Y. Mao and Y. Zhang, Chem. Phys. Lett. **542**, 37 (2012).
[35] P. Debenedetti, J. Phys. Condens. Matter **15**, R1669 (2003).
[36] A. K. Soper, Chem. Phys. **258**, 121 (2000).
[37] I. M. Svishchev and P. G. Kusalik, J. Phys. Chem. **98**, 728 (1994).
[38] M. Shiga and W. Shinoda, J. Chem. Phys. **123**, 134502 (2005); W. Shinoda and M. Shiga, Phys. Rev. E **71**, 041204 (2005).
[39] C. Vega, M. Conde, C. McBride, J. Abascal, E. Noya, R. Ramirez, and L. Sesé, J. Chem. Phys. **132**, 046101 (2010).
[40] J. Lobaugh and G. A. Voth, J. Chem. Phys. **106**, 2400 (1997).
[41] M. Lísal, W. Smith, and K. Aim, Mol. Phys. **101**, 2875 (2003).
[42] H. Pfeiffer and K. Heremans, ChemPhysChem **6**, 697 (2005).
[43] S. Santucci, D. Fioretto, L. Comez, A. Gessini, and C. Masciovecchio, Phys. Rev. Lett. **97**, 225701 (2006).
[44] T. Ikeda, Y. Katayama, H. Saitoh, and K. Aoki, J. Chem. Phys. **132**, 121102 (2010).
[45] G. Weck, J. Eggert, P. Loubeyre, N. Desbiens, E. Bourasseau, J.-B. Maillet, M. Mezouar, and M. Hanfland, Phys. Rev. B **80**, 180202(R) (2009).
[46] D. Kang, J. Dai, and J. Yuan, J. Chem. Phys. **135**, 024505 (2011).
[47] S. F. O'Shea and P. R. Tremaine, J. Phys. Chem. **84**, 3304 (1980).